JOURNAL OF GUIDANCE, CONTROL, AND DYNAMICS
Vol. 39, No. 12, December 2016

Continuous-Time Modeling and Control Using Nonsingular Linearized Relative-Orbit Elements

Trevor Bennett* and Hanspeter Schaub†
University of Colorado, Boulder, Colorado 80309

DOI: 10.2514/1.G000366

Applications, such as autonomous rendezvous and docking for CubeSats, on-orbit assembly of space stations, and orbital-debris harvesting or removal technologies, require relative-motion guidance-and-control-approach application for close-proximity operations with frequent trajectory controls. This study expands upon current relative-orbit approaches in delivering a nonsingular osculating linearized-relative-orbit-element state extracted from the Clohessy–Wiltshire equations' integration constants capable of including perturbation accelerations and control. The Lagrangian brackets, used in Lagrange's planetary equations and other osculating forms, are applied to the acquired state vector to obtain the elegantly simple kinematics. The proposed relative-motion state vector is promising for a range of proximity operations, as it provides the capability to include perturbation accelerations and control without altering the formulation and no loss of geometric insight. The linearized-relative-orbit-element variational equations are validated with a differential drag example. The Lyapunov control theory is applied to develop a linearized-relative-orbit-element feedback-control law demonstrating transitioning between relative orbits. The linearized-relative-orbit-element control formulation is implemented for two relative-orbit reconfigurations illustrating the geometric insight inherent in the developed approach.

I. Introduction

CLOSE-PROXIMITY relative-orbit control has applications in fractionated satellite formations, rendezvous and docking, and relative-motion sensing and estimation missions. Close-proximity maneuvering, sometimes as close as tens of meters, is a control-dominated environment where the primary sources of error are from relative sensing and thrust inaccuracies. Long-term propagation accuracy is not as critical as having simple to implement and effective guidance, navigation, and control (GNC) algorithms. Investigation into improving relative-motion GNC methods is further encouraged by the growing utilization of small satellites, CubeSats, and large constellations and formations [1]. One such representative mission is the NASA CubeSat Proximity Operation Demonstrator (CPOD) autonomous docking technology demonstrator [2,3]. The CPOD mission maneuvers a three-unit CubeSat pair through a low Earth orbit (LEO) relative approach from hundreds of meters down to multiple meter separation, including docking, to demonstrate the feasibility of autonomous circumnavigation maneuvers on modern CubeSat platforms. In such close-proximity operations where the chaser satellite is circumnavigating only tens of meters apart, small orbit corrections will frequently be required to account for sensor and thruster errors. In addition, the close-proximity relative motion between control updates is strongly dominated by the Keplerian relative-motion solution.

The close-proximity GNC approaches are also applicable for several touchless orbital-debris removal technologies being developed, including ion-sheppard [4–7], active eddy-current detumble [8], and electrostatic tugging [9–13]. In all these scenarios, the servicer and debris objects are flying only 2–10 craft radii apart and will require continuous station keeping. Here, electrostatic, magnetic, or ion control force is of the order of the differential gravity force, and perturbed relative motion is well modeled with a linearized gravity-field model. Additional close-proximity mission concepts flying only a few craft-radii apart are being considered for satellite component harvesting (Defense Advanced Research Projects Agency Phoenix), or on-orbit servicing and refueling [14]. Debris and servicing-related missions benefit from continuous feedback control to address the short-term mission-critical operations in the presence of perturbations and modeling errors. The reference trajectories of these proximity missions, including the CPOD mission, are composed of several relative-orbit reconfigurations to transition between safety ellipses, V-bar, and additional mission-relevant relative-motion segments. In all these cases, having a relative-motion description that is geometrically insightful facilitates planning and implementing these reconfiguration and close station-keeping maneuvers.

The choice of relative-motion kinematics can help simplify the feedback-control development, or can more easily visualize the perturbed relative-motion geometry due to disturbances, such as ion exhaust, magnetic actuation, or electrostatic tugging. A relative-orbit element, or ROE, is defined as the state obtained by differencing the orbits of the considered spacecraft. Several spacecraft missions, particularly on small and CubeSat missions, are already notable implementation ROE control schemes [15–17]. A group of research considers describing the relative motion through differencing of inertial orbit elements [18–20]. The benefit here is that these kinematics can scale to elliptical orbits and larger separation distances. However, the description requires a complex kinematic chain, in which the inertial position and velocity are mapped through the Earth coordinate frame to yield orbit-element differences describing the local relative motion. Another promising kinematic approach is to use inertial differencing of the eccentricity and inclination vectors, as has been applied to the PRISMA mission [21,22]. Here, too, inertial orbit quantities are differenced to obtain the relative motion.

In contrast, linearized solutions, including the Clohessy–Wiltshire (CW) equations, were developed to assist in Gemini's rendezvous and docking missions [23]. The CW equations are applicable for circular chief orbits and small separation distances. The CW equations receive significant attention due to the number of space assets that operate in circular, or near-circular, orbits. The geostationary belt (GEO) and the International Space Station are two of the most notable circular orbits that experience significant formation flying, rendezvous and docking, and proximity operations. CubeSat missions, which are often injected into circular LEO orbits as secondary payloads, also constitute a growing market for relative-motion control. The CW equations describe the motion using time-varying Cartesian or curvilinear

Received 24 December 2015; revision received 5 May 2016; accepted for publication 22 June 2016; published online 6 October 2016.

*Graduate Research Assistant, Aerospace Engineering Sciences. Student Member AIAA.

†Alfred T. and Betty E. Look Professor of Engineering, Associate Chair of Graduate Affairs, Department of Aerospace Engineering Sciences, 431 UCB, Colorado Center for Astrodynamics Research.

coordinates, and have an elegant analytical closed-form solution of the linearized relative motion [23]. This relative-motion solution is insightful in determining the geometry of the relative motion. New solutions to the linearized relative motion continue to be developed using both rectilinear and curvilinear state spaces [24–27]. In particular, in 2004, Lovell et al. proposed using some of the integration constants of the CW relative-motion solution as the ROE elements as control variables. The control of these ROEs is demonstrated via Hill-frame impulsive velocity changes [26], or continuous on–off thruster solutions [28]. The relative-motion geometry is discussed in detail by Lovell and Spencer in [29]. An excellent technical report of ROEs as integration constants of relative motion and control formulations is presented by D'Amico in [30].

There is a rich literature on ROEs that focuses either on the differential orbit-element formulations [19,31–33] on the eccentricity/inclination-vector-difference formulation [27,30,34], and using integration constants of the CW solution [25,35,36]. This paper expands on the work that considers a relative-motion description based on the CW integration constants. The earlier work by Lovell and Tragesser in [25] considers subsets of the CW integration constants as linearized relative-orbit elements (LROEs). However, although these coordinates do provide elegant geometric insight, not all are invariants of the unperturbed relative motion. The control in these formulations, as well as follow-on work [37], is implemented via impulsive Hill-frame velocity changes. Recent work by Spencer illustrates the use of these LROEs to perform relative-orbit targeting with artificial potential functions [36]. Of concern, these LROEs are also singular for particular relative-motion types, like the lead–follower formation. Ichimura and Ichikawa investigate in [35] using CW invariants to control the relative-orbit geometry impulsively. The invariants chosen are also singular for lead–follower and in-plane formations, same as with the LROE in [25], and no variational equations of these CW invariants are developed.

This paper investigates describing and controlling the relative motion using a set of six singular CW integration constants presented in 2003 in [38], as well as nonsingular variations thereof. The original linearized relative motion is described in terms of in-plane and out-of-plane cyclic-motion amplitudes, phase angles, as well as along-track and radial offsets. As with the related CW invariant relative-motion descriptions earlier, the in-plane phase angle is singular for the lead–follower formulation, and the out-of-plane phase angle is singular for planar motions. Of interest is how the original CW equations can be modified to yield a nonsingular LROE formulation, and find the associated variational equations. For example, having LROE kinematics with continuous perturbations is required when modeling the influence of magnetic, electrostatic, or thruster-plume-based formation flying. Using LROEs here is convenient in that they readily describe the current osculating relative-orbit geometry. The CW invariants used by Ichimura and Ichikawa [35], discussed previously, are closely related geometric parameters to the singular invariants used in [38]. In contrast to the earlier work, developing nonsingular variational equations of CW invariants allows for continuous control or perturbation influences to be included. Vallado [39] provides an elegant nonsingular CW solution in terms of the initial Cartesian Hill-frame position and velocity coordinates. These initial conditions are invariants of the unperturbed linearized relative motion, but do not provide any geometric insight into the resulting relative orbit. This paper investigates new variational equations for both singular and nonsingular CW invariant formulations based on the LROE discussed in [38]. The use of these particular LROE formulations is illustrated by studying how differential atmospheric drag perturbs the relative-orbit shape. The shape changes are readily apparent in the LROE states, thanks to their geometric interpretation. Further, to illustrate how LROE-based control solutions can be developed with the associated variational equations, the Lyapunov theory is employed to develop a relative-orbit tracking control. A large relative-orbit shape-reconfiguration maneuver is investigated and studied with numerical simulations. This control is analogous to how Gauss's variational equations are used to derive Lyapunov-based inertial orbit control solutions [40], but applied to the LROE variational equations.

II. Linearized Relative-Orbit Elements

The relative motion of the considered ROEs is derived in the Hill frame defined in Fig. 1. The Hill frame is defined by $\mathcal{H} = \{\hat{\boldsymbol{o}}_r, \hat{\boldsymbol{o}}_\theta, \hat{\boldsymbol{o}}_h\}$, in which $\hat{\boldsymbol{o}}_r$ is aligned with the reference craft orbit radius, $\hat{\boldsymbol{o}}_h$ is aligned with the reference craft orbit angular momentum, and $\hat{\boldsymbol{o}}_\theta$ completes the orthonormal reference frame. The deputy spacecraft motion is described relative to a chief reference craft. The focus of this work is the reduction of the relative-orbit problem to the CW equations that describe the motion of the deputy about a circular reference orbit. The linearized relative equations of motion of a deputy about a circular chief are given by [23]

$$\ddot{x} - 3n^2x - 2n\dot{y} = a_x \tag{1a}$$

$$\ddot{y} + 2n\dot{x} = a_y \tag{1b}$$

$$\ddot{z} + n^2z = a_z \tag{1c}$$

For unperturbed Keplerian motion, the inertial acceleration components a_x, a_y, and a_z are set to zero, allowing this differential relative-motion equation to be analytically integrated [23,38].

$$x(t) = A_0\cos(nt + \alpha) + x_{\text{off}} \tag{2a}$$

$$y(t) = -2A_0\sin(nt + \alpha) - \frac{3}{2}ntx_{\text{off}} + y_{\text{off}} \tag{2b}$$

$$z(t) = B_0\cos(nt + \beta) \tag{2c}$$

The preceding formulation is taken from [38], in which A_0 is the amplitude measure of the in-plane cyclic component, B_0 is the magnitude out-of-plane cyclic component, α and β are the respective phase angles of the cyclic motions, x_{off} is the static radial offset, and y_{off} is the along-track offset at the epoch time. Other integration constants could have been chosen, such as the Hill-frame Cartesian initial conditions [39], or drift rates instead of x_{off}, such as in [35]. Naturally, there are direct transformations between all these sets of CW invariants. However, each CW set has its own advantages regarding simplicity of implementation, singular behavior, or geometric insight.

Using these LROE invariants of the unperturbed CW equations, the Hill-frame velocity coordinates are expressed as

$$\dot{x}(t) = -A_0n\sin(nt + \alpha) \tag{3a}$$

$$\dot{y}(t) = -2A_0n\cos(nt + \alpha) - \frac{3}{2}nx_{\text{off}} \tag{3b}$$

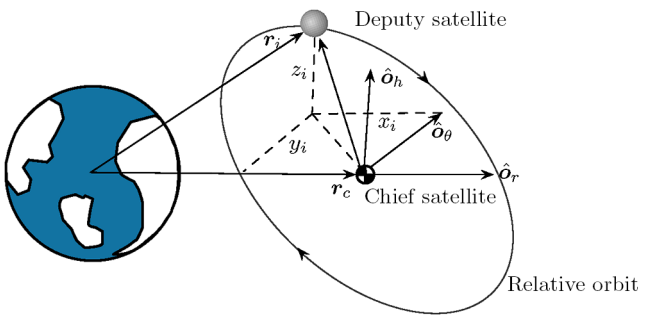

Fig. 1 Local-vertical/local-horizontal rotating Hill frame for formation flying [38].

$$\dot{z}(t) = -B_0 n \sin(nt + \beta) \tag{3c}$$

The CW equations provide a convenient form for directly prescribing the relative orbit, and are often used for geometric insight of the relative-orbit shape. The magnitudes of the scaling and phasing terms enable the direct shaping of the relative orbit. It is the geometrically intuitive nature of these constants that motivates the following development. The relative position described by Eq. (2) is limited by the underlying assumption to neglect perturbation accelerations allowing constants to appear in the CW equations as invariants of the unperturbed linearized motion. This work considers the invariants as a set of ROEs and develops the necessary osculating state dynamics to reintroduce perturbation accelerations. As this set of ROEs is derived from the linearized motion solution, the invariant vector of the CW equations is referred to as an LROE.

Taken at the epoch time, the invariants of motion $A_0, \alpha, B_0, \beta, x_{\text{off}}$, y_{off}, and the CW solution provide a position and velocity of the deputy spacecraft about the circular chief orbit. The Cartesian and LROE state vectors are

$$\boldsymbol{s} = [x \quad y \quad z \quad \dot{x} \quad \dot{y} \quad \dot{z}]^T = \begin{bmatrix} \boldsymbol{r} \\ \boldsymbol{v} \end{bmatrix} \tag{4a}$$

$$\boldsymbol{\alpha} = [A_0 \quad \alpha \quad x_{\text{off}} \quad y_{\text{off}} \quad B_0 \quad \beta]^T \tag{4b}$$

An inverse mapping between a Cartesian state $\boldsymbol{s}$ and the LROEs is obtained in Eq. (5), in which the current mean motion and time of the chief spacecraft are used:

$$A_0 = \frac{\sqrt{9n^2x^2 + \dot{x}^2 + 12nx\dot{y} + 4\dot{y}^2}}{n} \tag{5a}$$

$$\alpha = \tan^{-1}\left(\frac{-\dot{x}}{-3nx - 2\dot{y}}\right) - nt \tag{5b}$$

$$x_{\text{off}} = 4x + 2\frac{\dot{y}}{n} \tag{5c}$$

$$y_{\text{off}} = -2\frac{\dot{x}}{n} + y + (6nx + 3\dot{y})t \tag{5d}$$

$$B_0 = \frac{\sqrt{n^2z^2 + \dot{z}^2}}{n} \tag{5e}$$

$$\beta = \tan^{-1}\left(\frac{-\dot{z}}{nz}\right) - nt \tag{5f}$$

The inverse mapping allows the LROEs to be obtained at any point in time given the relative motion of the system as mapped from the CW Hill frame to the LROE space. Consider the CW equations in Eq. (1) and the inverse mapping in Eq. (5). If the elliptical invariant A_0 or B_0 is zero in Eq. (1), then the angles α and β are ambiguous. In addition, the inverse mapping introduces an inverse tangent function that is subject to singularities and the secular term nt that must be modulo 2π for consistency over longer time spans. The inverse-mapping epoch time is a free variable and can be chosen as the most convenient time or reset throughout operation to combat secular growth in the terms. The free time variable is inherited from the CW equations, in which an epoch is chosen, and the phasing and coefficients are computed to match the epoch state. This mapping is required unless additional logic is included or further reduced forms of the equations are used. The CW equations, therefore, are unable to provide a unique solution to the leader–follower configuration without modification. These singularities in the CW form motivate alternate or modified forms of the CW equations and invariant set.

III. Nonsingular Modification to the LROE Set

The preceding singularities of the CW invariants presented in [33,38] are addressed by a new LROE formulation. Note that these new nonsingular LROEs can also be applied to the relative-motion kinematics being developed by [25,29]. Ambiguities and singularities arise with the two phase angles α and β for particular relative-orbit geometries. To remove these issues, the following trigonometric expansions are used:

$$A_0 \cos(\alpha + nt) = A_0 \cos(\alpha)\cos(nt) - A_0 \sin(\alpha)\sin(nt) \tag{6a}$$

$$A_0 \sin(\alpha + nt) = A_0 \sin(\alpha)\cos(nt) + A_0 \cos(\alpha)\sin(nt) \tag{6b}$$

in which new LROE parameters A_1 and A_2 are defined as

$$A_1 = A_0 \cos(\alpha) \tag{7a}$$

$$A_2 = A_0 \sin(\alpha) \tag{7b}$$

which replace the singular A_0 and α parameter set. The ambiguity of the linear combination of A_0 and α is removed in place of two perpendicular scaling terms. Similarly, the new nonsingular out-of-plane LROEs are defined as

$$B_1 = B_0 \cos(\beta) \tag{8a}$$

$$B_2 = B_0 \sin(\beta) \tag{8b}$$

Using the simplifications in Eqs. (6a) and (7a), the new CW solution is rewritten into the proposed nonsingular LROE form as

$$x(t) = A_1 \cos(nt) - A_2 \sin(nt) + x_{\text{off}} \tag{9a}$$

$$y(t) = -2A_1 \sin(nt) - 2A_2 \cos(nt) - \frac{3}{2}ntx_{\text{off}} + y_{\text{off}} \tag{9b}$$

$$z(t) = B_1 \cos(nt) - B_2 \sin(nt) \tag{9c}$$

The time derivative of the modified CW solution provides the relative-motion rates.

$$\dot{x}(t) = -A_1 n \sin(nt) - A_2 n \cos(nt) \tag{10a}$$

$$\dot{y}(t) = -2A_1 n \cos(nt) + 2A_2 n \sin(nt) - \frac{3}{2}nx_{\text{off}} \tag{10b}$$

$$\dot{z}(t) = -B_1 n \sin(nt) - B_2 n \cos(nt) \tag{10c}$$

The new LROE set is of all in units of distance providing additional implementation simplicity.

$$\boldsymbol{\alpha} = [A_1 \quad A_2 \quad x_{\text{off}} \quad y_{\text{off}} \quad B_1 \quad B_2]^T \tag{11}$$

Whereas the earlier LROEs contained both distance and angle measures, the nonsingular LROEs only contain distance measures. The LROEs defined in Eq. (11) are obtained from Cartesian Hill frame states through the following inverse mapping:

$$A_1 = -\frac{(3nx + 2\dot{y})\cos(nt) + \dot{x}\sin(nt)}{n} \tag{12a}$$

$$A_2 = \frac{(3nx + 2\dot{y})\sin(nt) - \dot{x}\cos(nt)}{n} \tag{12b}$$

$$x_{\text{off}} = 4x + \frac{2\dot{y}}{n} \tag{12c}$$

$$y_{\text{off}} = -\frac{2\dot{x}}{n} + y + (6nx + 3\dot{y})t \tag{12d}$$

$$B_1 = z\cos(nt) - \frac{\dot{z}\sin(nt)}{n} \tag{12e}$$

$$B_2 = -z\sin(nt) - \frac{\dot{z}\cos(nt)}{n} \tag{12f}$$

The analytic inverse allows Hill-frame measurements to be easily mapped into LROE information.

Similar to the singular LROE set, the modified LROE inverse mapping has time as a free variable. The ability to set t to any desired epoch may introduce improvement or degradation in relative-orbit reconfiguration. The reconfiguration from one LROE set to another represents the reconfiguration between two relative orbits with respective phasing. If the phasing is not a constrained parameter, then the time parameter may be selected for the most cost-efficient transfer between two relative-orbit geometries [35]. In contrast to the inverse mapping of the classical LROEs, the nonsingular LROE mapping from Cartesian states is free of singularities. This allows these LROEs to readily describe or control the relative orbit for any relative trajectory shape.

IV. Lagrangian-Bracket Development of LROE Variational Equations

A. Overview of Variational-Equation Development

Gauss's variational equation is a classic result that shows how invariants of the unperturbed motion (i.e., inertial orbit elements) will vary in the presence of perturbation accelerations [41]. This section derives the analogous variational equations for both the classical and new nonsingular LROEs. The Lagrangian-bracket methodology evolves the invariants of motion present in a dynamic system's analytical solution to match the perturbed solution at the prescribed time. Given the inverse mappings provided in Eqs. (5) and (12), the sensitivity matrices are computable. The LROE set $\boldsymbol{\alpha}$, otherwise invariant, evolves according to [38]

$$\dot{\boldsymbol{\alpha}} = [L]^{-1}\left[\frac{\partial \boldsymbol{r}}{\partial \boldsymbol{\alpha}}\right]^T \boldsymbol{a}_d \tag{13}$$

in which $\boldsymbol{r}$ is the deputy position vector, and $\boldsymbol{a}_d$ is the disturbance acceleration. The Lagrangian-bracket matrix $[L]$ is defined by

$$[L] = \frac{\partial \boldsymbol{s}}{\partial \boldsymbol{\alpha}}^T [J] \frac{\partial \boldsymbol{s}}{\partial \boldsymbol{\alpha}} \tag{14}$$

and $[J]$ is the symplectic matrix. A full description of the Lagrangian-bracket methodology is included in chapter 12 of [38]. The equations of motion for the LROEs in Eq. (13) are simplified by defining the control matrix $[B]$ as

$$[B] = [L]^{-1}\left[\frac{\partial \boldsymbol{r}}{\partial \boldsymbol{\alpha}}\right]^T \tag{15}$$

allowing the LROE equations of motion to assume the following familiar dynamics form:

$$\dot{\boldsymbol{\alpha}} = [B]\boldsymbol{u} \tag{16}$$

This algebraic expression is similar to Gauss's variational equations for inertial orbit elements, which is heavily used in perturbation and control studies. Applying this derivation approach to the invariants of the linearized relative motion will lead to the desired LROE variational equations.

B. Classic LROE Variational Equations of Motion

First, the variational equations of the original LROEs in Eq. (4b) are developed. The necessary partials for Eq. (14) are developed by first defining the simplifying terms:

$$\kappa_\alpha = nt + \alpha \qquad \kappa_\beta = nt + \beta \tag{17}$$

Utilizing the κ_α and κ_β definitions, the partial derivatives of the relative position vector with respect to the classic LROEs are

$$\frac{\partial \boldsymbol{r}}{\partial \boldsymbol{\alpha}} = \begin{bmatrix} \cos(\kappa_\alpha) & -A_0\sin(\kappa_\alpha) & 1 & 0 & 0 & 0 \\ -2\sin(\kappa_\alpha) & -2A_0\cos(\kappa_\alpha) & -\frac{3}{2}nt & 1 & 0 & 0 \\ 0 & 0 & 0 & 0 & \cos(\kappa_\beta) & -B_0\sin(\kappa_\beta) \end{bmatrix} \tag{18}$$

Similarly, taking the partials of $\boldsymbol{r}$ in Eq. (2) and $\boldsymbol{\nu}$ in Eq. (3) with respect to the LROE set in Eq. (4b) yields the following Lagrangian-bracket-matrix components:

$$\begin{aligned} L_{1,2} &= -5A_0 n & L_{2,4} &= -2A_0 n\sin(\kappa_\alpha) \\ L_{1,3} &= -3n^2 t\cos(\kappa_\alpha) + 4n\sin(\kappa_\alpha) & L_{3,4} &= 3n/2 \\ L_{1,4} &= 2n\cos(\kappa_\alpha) & L_{5,6} &= -B_0 n \\ L_{2,3} &= A_0 n[4\cos(\kappa_\alpha) + 3nt\sin(\kappa_\alpha)] & & \end{aligned} \tag{19}$$

The sparsely populated $[L]$ is presented in component form, in which the skew-symmetric property is required to build the full matrices. Inserting the inverse of Eq. (19) and the partials in Eq. (18) into Eq. (15) yields the desired classic LROE variational-equation $[B]$ matrix.

$$[B]_{\text{classic}} = \frac{1}{n}\begin{bmatrix} -\sin(\kappa_\alpha) & -2\cos(\kappa_\alpha) & 0 \\ -\cos(\kappa_\alpha)\frac{1}{A_0} & 2\sin(\kappa_\alpha)\frac{1}{A_0} & 0 \\ 0 & 2 & 0 \\ -2 & 3nt & 0 \\ 0 & 0 & -\sin(\kappa_\beta) \\ 0 & 0 & -\cos(\kappa_\beta)\frac{1}{B_0} \end{bmatrix} \tag{20}$$

As expected, the $\dot{\alpha}$ and $\dot{\beta}$ evaluations are singular if the A_0 and B_0 parameters are, respectively, zero.

Naturally, all the linearized relative-motion variational equations must be related to other dynamic forms, as they describe the same physical relative trajectory. For example, using Eq. (20) yields

$$\dot{x}_{\text{off}} = \frac{2}{n}a_y \tag{21}$$

The orbit-element-difference-based ROE variational equations used in [18] can be related to these classical LROE variational equations. For example, note that $x_{\text{off}} = \delta a$ [33]. Thus, assuming a circular unperturbed chief orbit and using Gauss's variational equations [41], the x_{off} variational equation must be

$$\dot{x}_{\text{off}} = \delta\dot{a} = \dot{a} = \frac{2a^2}{h}a_y = \frac{2}{n}a_y \tag{22}$$

However, other LROE elements have a more complex relationship to the inertial orbit-element differences, such as $B_0 = a\sqrt{\delta i^2 + \sin^2 i\delta\Omega^2}$ or the phase angles α and β. In this case, the process of taking the time derivative and applying Gauss's variational

equations is not as straightforward. The presented Lagrangian-bracket approach is elegant in that it uses the analytical CW formulation directly and does not require the use of the Gauss's variational equations as a subresult.

C. Modified LROE Lagrangian-Bracket Development

Next, the nonsingular LROE set defined in Eq. (11) is considered. Following the same approach used to develop the Lagrangian brackets for the classical CW form, this section develops the Lagrangian brackets for the modified LROEs. Taking the partials of the CW state in Eq. (9) with respect to the nonsingular LROEs yields

$$\frac{\partial \boldsymbol{r}}{\partial \boldsymbol{\alpha}} = \begin{bmatrix} \cos(nt) & \sin(nt) & 1 & 0 & 0 & 0 \\ -2\sin(nt) & -2\cos(nt) & -3/2nt & 1 & 0 & 0 \\ 0 & 0 & 0 & 0 & \cos(nt) & -\sin(nt) \end{bmatrix} \tag{23}$$

$$\begin{aligned} L_{1,2} &= -5n & L_{2,4} &= -2n\sin(nt) \\ L_{1,3} &= -3n^2 t\cos(nt) + 4n\sin(nt) & L_{3,4} &= 3n/2 \\ L_{1,4} &= 2n\cos(nt) & L_{5,6} &= -n \\ L_{2,3} &= 4n\cos(nt) + 3n^2 t\sin(nt)] \end{aligned} \tag{24}$$

Again, the sparsely populated and skew-symmetric matrix $[L]$ is presented in component. Inserting the inverse of Eq. (24) and the partials in Eq. (23) into Eq. (15) for the modified state vector in Eq. (11) gives the modified LROE $[B]$ matrix:

$$[B]_{\text{modified}} = \frac{1}{n}\begin{bmatrix} -\sin(nt) & -2\cos(nt) & 0 \\ -\cos(nt) & 2\sin(nt) & 0 \\ 0 & 2 & 0 \\ -2 & 3nt & 0 \\ 0 & 0 & -\sin(nt) \\ 0 & 0 & -\cos(nt) \end{bmatrix} \tag{25}$$

It can also be shown that the Poisson-bracket approach confirms the Lagrangian-bracket forms presented. Note that, with these variational equations, the denominators can never go to zero, yielding a nonsingular LROE variational equation. This elegantly simple $[B]_{\text{modified}}$ matrix allows for the geometrically insightful LROE to be used as control variables, or to study the impact of a continuous disturbance, such as drag or Lorentz forces, would have on the relative-orbit geometry.

V. Perturbation Effects Present in Modified LROEs

Next, the impact of differential atmospheric drag on the relative-orbit geometry is investigated with the nonsingular LROEs. This section provides a numerical validation of the analytical variational LROE equations by comparing them to the full nonlinear solution. Further, it provides an illustrative example how a continuous disturbance will vary the LROE parameters, providing insight into how the relative-orbit geometry varies. Consider the influence of drag on a spacecraft defined by the drag acceleration expression:

$$\ddot{\boldsymbol{r}} = -\frac{1}{2}C_D\frac{A}{m}\rho_A\|\boldsymbol{V}_A\|\boldsymbol{V}_A \tag{26}$$

The drag-model parameters assume the following density model:

$$\rho_A = \rho_0 e^{-(r-r_0)/H} \tag{27}$$

in which the reference atmospheric density is $\rho_0 = 3.614 \times 10^{-13}$ km/m^3, the reference radius is $r_0 = (700\text{ km} + R_{\text{Earth}})$, and the scaling height is $H = 88.6670$ km. The contribution from the rotation of the Earth's atmosphere includes the Earth spin rate. Drag is applied to each spacecraft in the full nonlinear numerical analysis initialized an equatorial circular LEO chief with a semimajor axis of $a = 6778$ km. The simulated inertial state is composed of position and velocity for both uncontrolled chief spacecraft and deputy spacecraft. The simulations are propagated for a duration of 10 chief orbits at $\Delta t = 0.5$ s with drag as the only non-Keplerian perturbation. The chief is given a $C_D = 2.0$ with a representative area of $A = 3$ m^2 and mass of 970 kg. The deputy differs only with a drag coefficient of $C_D = 2.2$.

In this illustrative example, the influence of the described drag model is considered in a planar-ellipse spacecraft formation defined by the initial modified LROE set:

$$\begin{aligned} \boldsymbol{\alpha}_0 &= [A_{1,0} \quad A_{2,0} \quad x_{\text{off},0} \quad y_{\text{off},0} \quad B_{1,0} \quad B_{2,0}]^T \\ &= [20 \quad 0 \quad 0 \quad 0 \quad 0 \quad 0][\text{m}] \end{aligned}$$

Figure 2 reflects the effect of drag on the relative-orbit geometry by visualizing the solution of the nonlinear simulation by mapping the inertial simulation states to their equivalent LROE values. The LROE parameters shown are extracted at each time step using the inverse mapping provided. The out-of-plane B_1 and B_2 parameters remain zero and are not shown. Notable are the x_{off} error in Fig. 2c and the y_{off} error in Fig. 2d. As expected, the nonzero value and secular growth of x_{off} shears the relative motion apart with the y_{off} trend diverging from a bounded formation. However, the cyclic in-plane motion, described through A_1 and A_2, only undergoes periodic osculating variations without any secular growth.

Next, the simulation is repeated using the LROE variational equations, and compared to the inertial simulation result to validate the expressions found. The differential drag of the two spacecraft expressed in the Hill frame is introduced as a disturbance acceleration to evolve the LROEs over several orbits. The predictive model computes the instantaneous velocity of both the deputy and the chief using the initial chief epoch, the current time, and the instantaneous LROEs. The differential drag on the formation is achieved by differencing the acceleration due to drag on the respective spacecraft as expressed in the Hill frame. The errors between the nonsingular variational LROE simulation and the inertial simulation are shown in Fig. 3. Only the first five orbits are shown to better discern the detail near initialization and before the Δy_{off} grows significantly. The drag-perturbed relative-motion prediction matches well over the first few orbits with initial errors on the order of 0.1 mm. This numerically validates the derived LROE variational equations. However, over the course of 10 orbits, the estimate of the x_{off} grows due to the linearization errors and further drives the y_{off} away from the truth. The relative-orbit size described by A_1 and A_2 is submillimeter in accuracy initially, and then grows in sinusoidal fashion as the position error grows. The degradation of the estimate is expected due to the first-order approximation of the relative motion.

The classical LROE parameter variations of A_0 and α are shown in Fig. 4. The x_{off} and y_{off} elements have the equivalent mapping as the modified set. The ΔA_0 value in Fig. 4a is much larger than the nonsingular LROE ΔA_i errors over the first few orbits. The modified set combines the size, A_0, and phasing, α, into two terms that are orthogonal, enabling less prediction error.

Periodically reinitializing the LROEs can combat the growing errors in the LROEs due to linearization and reinjection. Recall that the LROEs are chosen at a specific epoch time, and so the LROEs could be recomputed from inertial estimates to provide several more orbits of acceptable prediction. It is important to note that inclusion of an eccentric chief craft reduces the validity of the LROE prediction model.

VI. Continuous-Feedback-Control Development

A continuous feedback control is employed if tight station keeping or trajectory tracking is required. Gauss's variational equations have been used extensively to derive inertial and differential orbit-element-based control strategies [18,40]. This section derives a Lyapunov-based feedback-control strategy, in which the deputy satellite assumed to be able to achieve a desired inertial control acceleration vector $\boldsymbol{u} = \boldsymbol{a}_d$ to drive the osculating LROEs toward a set of reference LROE states $\boldsymbol{\alpha}_r(t)$. Having $\boldsymbol{\alpha}_r$ varying with time

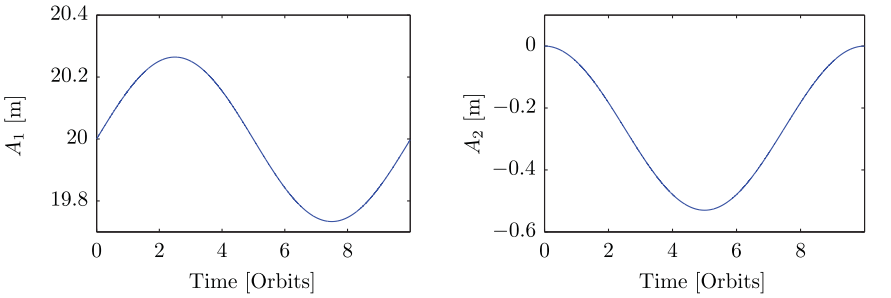

a) A_1 perturbed by drag b) A_2 perturbed by drag

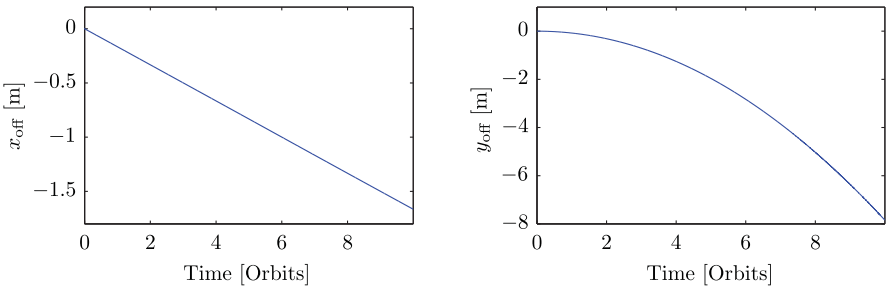

c) x_{off} perturbed by drag d) y_{off} perturbed by drag

Fig. 2 LROE evolution in the presence of drag.

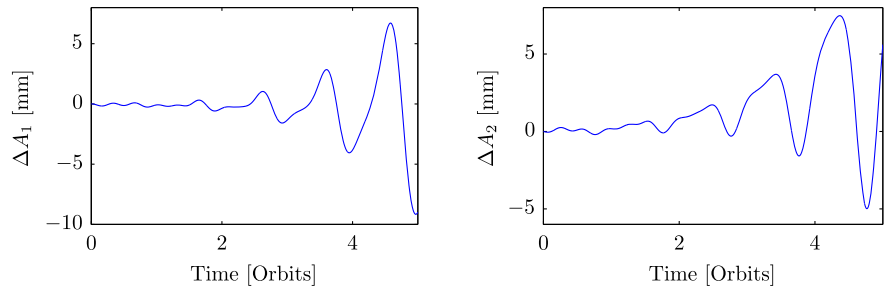

a) ΔA_1 - prediction error b) A_2 - prediction error

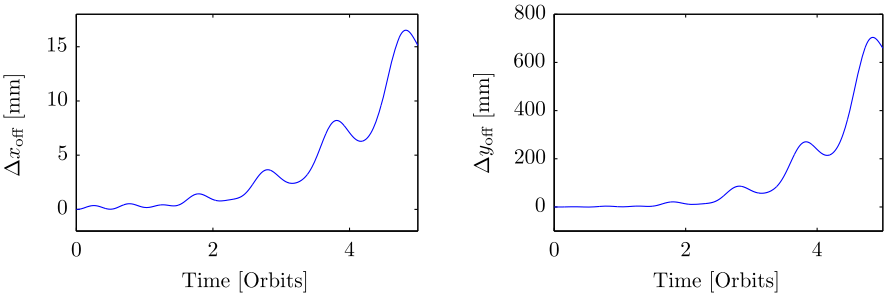

c) x_{off} - prediction error d) y_{off} - prediction error

Fig. 3 LROE prediction error in the presence of drag.

allows for unnatural circumnavigation solutions to be considered as well [42]. The LROE tracking-error measures are defined as

$$\Delta\boldsymbol{\alpha} = \boldsymbol{\alpha} - \boldsymbol{\alpha}_r \tag{28a}$$

$$\Delta\dot{\boldsymbol{\alpha}} = \dot{\boldsymbol{\alpha}} - \dot{\boldsymbol{\alpha}}_r = [B](\boldsymbol{u} - \boldsymbol{u}_r) \tag{28b}$$

A Lyapunov-based control approach is employed that follows the development of the mean orbit-element-difference control in [18]. The Lyapunov candidate function is defined as

$$V(\Delta\boldsymbol{\alpha}) = \frac{1}{2}\Delta\boldsymbol{\alpha}^T[K]\Delta\boldsymbol{\alpha} \tag{29}$$

in which $[K]$ is a 6×6 symmetric positive definite gain matrix. Taking the time derivative of the Lyapunov function and substituting the LROE variational equations yield

$$\dot{V}(\Delta\boldsymbol{\alpha}) = \Delta\boldsymbol{\alpha}^T[K][B](\boldsymbol{u} - \boldsymbol{u}_r) \tag{30}$$

The following LROE feedback-control law is proposed:

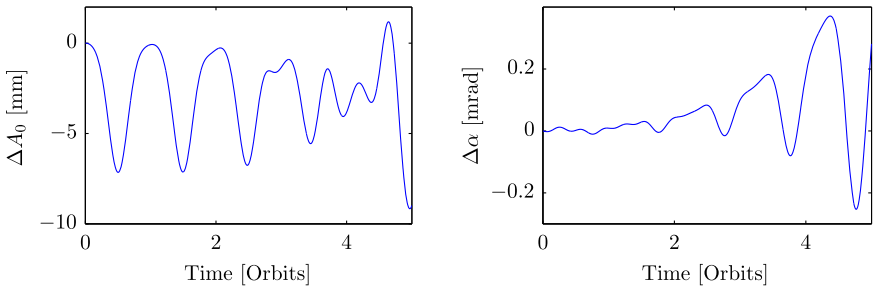

a) ΔA_o - prediction error **b) α - prediction error**

Fig. 4 Classic LROE prediction error in the presence of drag.

$$\boldsymbol{u} = \boldsymbol{u}_r - ([B]^T[B])^{-1}[B]^T[K]\Delta\boldsymbol{\alpha} \tag{31}$$

The resulting Lyapunov rate is

$$\dot{V}(\Delta\boldsymbol{\alpha}) = -\Delta\boldsymbol{\alpha}^T[K][B]([B]^T[B])^{-1}[B]^T[K]\Delta\boldsymbol{\alpha} = -\boldsymbol{y}^T([B]^T[B])^{-1}\boldsymbol{y} \tag{32}$$

in which $\boldsymbol{y} = [B]^T[K]\Delta\boldsymbol{\alpha}$. Note that $([B]^T[B])^{-1}$ is a symmetric positive definite 3×3 matrix. The Lyapunov time derivative defined in Eq. (32) is negative semidefinite guaranteeing Lyapunov stability. To prove asymptotic stability, the vector $\boldsymbol{y}$ must be shown to zero only when the LROE error is zero. Because the matrix $[K]$ is chosen to be positive definite, the term $[K]\Delta\boldsymbol{\alpha}$ is always nonzero if the error is nonzero. However, due to the state dependency of the $[B]$ matrix, there are instantaneous points in time, in which $\boldsymbol{y}$ is zero with nonzero LROE tracking error. Although the combination of $[B]^T[K]\Delta\boldsymbol{\alpha}$ may instantaneously go to zero, the largest invariant set, in which the product remains zero for all time, is in which $\Delta\boldsymbol{\alpha}$ is zero at which point the control effort is zero. Thus, LaSalle's invariance principle delivers asymptotic stability.

The LROE control form shares many similarities to the control implementation for orbit-element differences. Recall that the prescribed error form is an ROE difference of the linearized motion. Capitalizing on the parallels with orbit-element differences, many other control forms are available from orbit-element-difference-control literature with a few shown in chapter 14 of [38].

VII. Inertial Simulation Control Implementation

The proposed relative-orbit description and associated control law are assessed using an inertial orbit simulation solving the full nonlinear two-body problem. As motivating examples, large close-proximity relative maneuvers are required in the electrostatic tugging research for orbital servicing [43], as well as the proposed CubeSat-Proximity Operations Demonstrator mission [3]. The numerical analysis assumes Keplerian orbits with an equatorial circular LEO chief with a semimajor axis of $a = 7550$ km. The simulated inertial state is composed of position and velocity vectors for both uncontrolled chief spacecraft and controlled deputy spacecraft. The simulations are propagated for a duration of 10 chief orbits to fully illustrate the near-steady-state behavior. The sample LROE reconfigurations considered transfer from a planar ellipse to a lead–follower and back again. These cases demonstrate the breadth of the controller and target specific singularities or coupling effects that render the classical CW parameterization insufficient. Notice that the reference LROE states $\boldsymbol{\omega}_r$ are set to constant values for each case. This study restricts the relative orbits to small separation distances and demonstrates two planar reconfiguration cases. Both cases use full inertial nonlinear simulation at an integration time step of 0.5 s.

The use of the LROE state and LROE controller enables reconfiguration between a planar-elliptic relative orbit to lead–follower and back again. Recall that the current relative orbit and desired relative orbit are both described by an LROE set. The first case considered is the planar elliptic to the lead–follower. Desired is a transition from a zero offset 2-1 ellipse to a standoff distance in the along-track direction ahead of the chief. The second case considered is the return from the lead–follower back to the initialized planar ellipse. The initial conditions and reference for the second case are the swapped values for the first case. The lead–follower formation is defined through $y_{\text{off}} = 30$ m, whereas the 2-1 ellipse is defined via $A_1 = 20$ m. All other reference LROE values are zero. The feedback gain matrix $[K]$ is selected to be

$$[K] = n \cdot \text{diag}([1, 1, 30, 1, 1, 1]) \tag{33}$$

Note that the gain on x_{off} tracking errors is much larger than the other gains to ensure the bounded relative-motion condition (i.e., $x_{\text{off}} = 0$) is regained quickly.

The transfer between the initial and reference LROEs is dominantly achieved within three orbits. The Hill-frame reconfiguration is shown in Fig. 5, in which the planar ellipse to lead-follower relative orbit reconfiguration ends at the final lead-follower point. The return to the planar ellipse is shown where the final point resides on the 2-1 ellipse.

As can be seen in the Hill-frame reconfiguration to the lead–follower, the deputy satellite initially moves along an elliptical path as the along-track offset is increased. Over the following orbits, the ellipse shifts with slight expansion before contracting onto the reference point. By inspection, the size of the relative-motion ellipse initially grows prescribed by the coupling in the variational equations in the along-track position. The planar elliptic to the lead–follower is a planar reconfiguration, and, therefore, the decoupled out-of-plane motion remains zero. During the return to the 2-1 ellipse, the deputy initially shifts the along-track offset back toward the desired zero offset as the relative-orbit scaling term is driven to a slightly decreased value. Once the controller moves the along-track error into the vicinity of zero, the controller drives the scaling term toward the increased value required for the 2-1 relative ellipse. The darker-green-layered 2-1 ellipse demonstrates that, following the third orbit, the deputy does remain on the prescribed 2-1 ellipse.

The modified LROE time history provides additional insight into the reconfiguration. Shown in Fig. 6 are the time histories of the two scaling terms A_1 and A_2, as well as the along-track and radial offsets with colors corresponding to the respective reconfigurations in the Hill frame; Fig. 5. The simultaneous reconfiguration of the

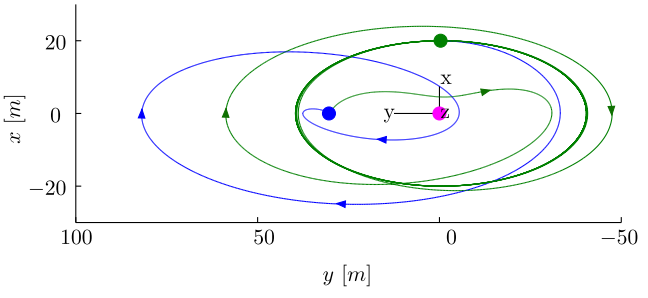

Fig. 5 Hill-frame reconfiguration between two relative orbit types.

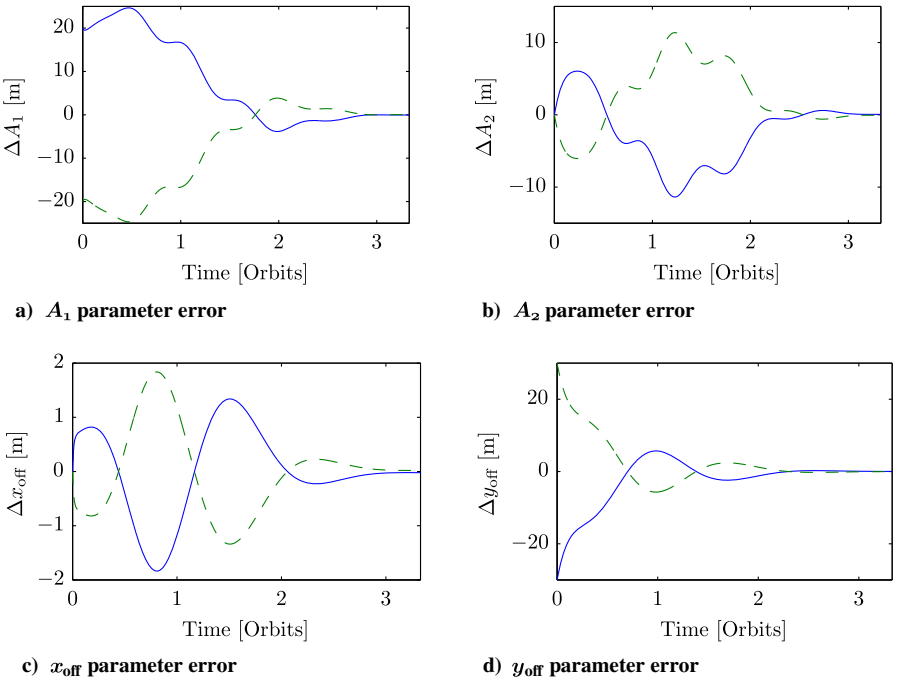

a) A_1 **parameter error** **b)** A_2 **parameter error**

c) x_{off} **parameter error** **d)** y_{off} **parameter error**

Fig. 6 LROE error for lead–follower to planar ellipse to lead–follower.

terms A_1 and y_{off} provides an interesting balance in the evolution of the relative orbit. Notably, the first half-orbit brings the x_{off} down and, therefore, the error up to sheer the deputy forward to the desired offset. The lightly damped but magnitude restricted response in x_{off} is due to the large gain placed on Δx_{off}. The current selection of a Δx_{off} error gain 30 times greater in magnitude than the other errors provides sufficient control authority without exceeding ± 2 m of offset. Additional tuning of the x_{off} term may provide a range of performance with the limits of divergence if the gain is zero and no control authority if the gain is infinite. The combination of the scaling terms provides a noticeable effect in the Hill-frame representation. Referring back to Fig. 5, the relative ellipse appears to rotate. This effect is attributed to the collective variation in A_1 and A_2 after the transition in offset. The greatest insight gained from the LROE errors in Fig. 6 is that the lead–follower to the elliptic evolution is the negative elliptic to the lead–follower. A strongly supported conclusion is that the trajectory between two relative orbits follows the same evolution of LROEs with only a sign difference in the forward and reverse reconfigurations. Such consistent evolution between two relative orbits is inherent in the Lagrange bracket formulation. This method then suggests that optimal reconfigurations may be obtained as a parameter sweep.

A logarithmic study of the LROE error shows the convergence behavior of the implemented control. Around the completion of three orbits, the controller is considered within sufficient accuracy of the reference location with additional convergence occurring over the following orbits. The logarithmic error for the LROEs is shown in Fig. 7. As claimed, the majority of the error is reduced after completion of three orbits. The humped variation in the A_1 and A_2 parameters corresponds directly to the half-orbit period.

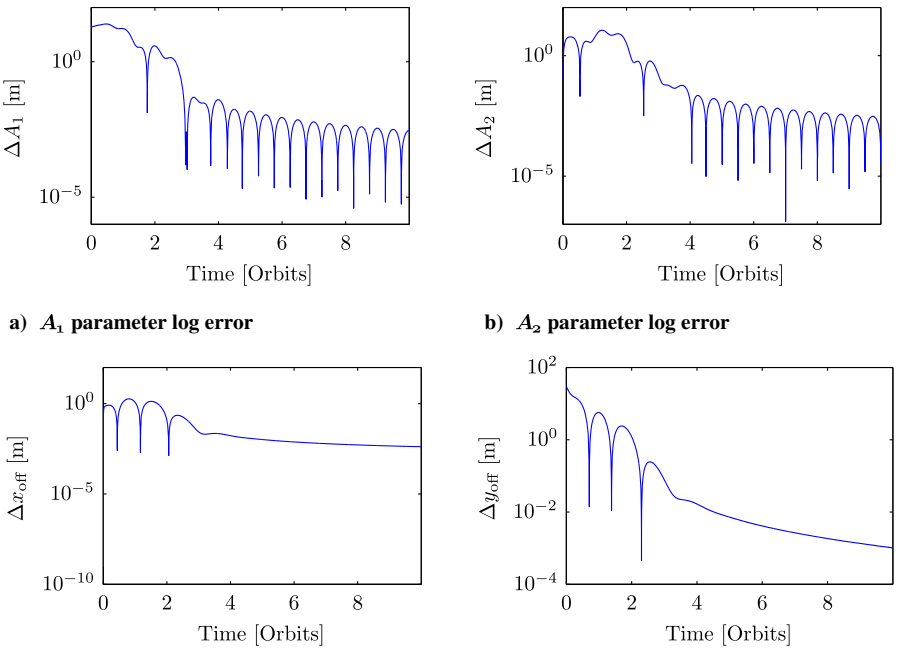

a) A_1 **parameter log error** **b)** A_2 **parameter log error**

c) x_{off} **parameter log error** **d)** y_{off} **parameter log error**

Fig. 7 Logarithmic LROE error for planar ellipse to lead–follower.

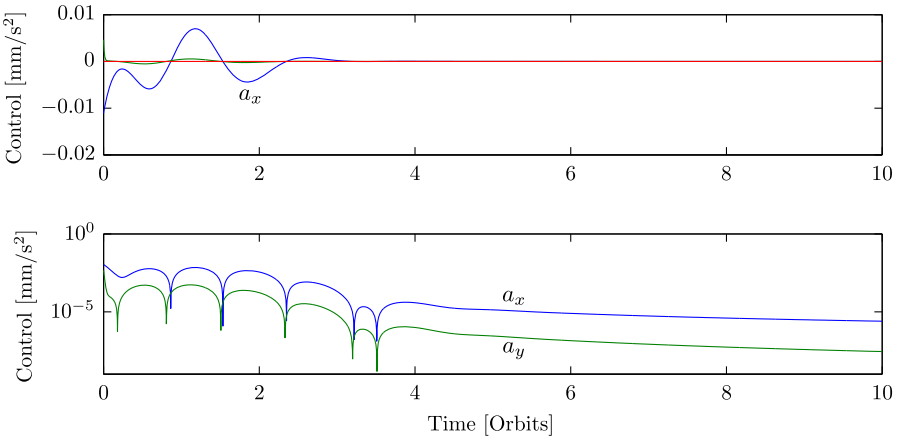

Fig. 8 Hill-frame deputy control effort from planar elliptic to lead–follower.

The errors presented in Fig. 7 are not expected to go to exactly zero. The LROE formulation is a first-order mapping with some errors incurred by the inverse mapping. Thus, the error obtained is near the best possible given the formulation and mapping equations. The Hill-frame control effort to produce the desired reconfiguration is shown in Fig. 8 on both linear and logarithmic scales to illustrate the transient and long-term effort. The top plot shows the first half of the reconfiguration, in which the bottom plot shows the logarithmic control effort. As can be seen in Fig. 8, the primary control effort is in the initial radial direction. This is expected because the y_{off} is controlled through the drift incurred by an x_{off}, and the A_1 scaling term is most dramatically reduced by the Hill x-direction acceleration. The slight y-direction acceleration is present with the direct impact requiring further study. The logarithmic control effort suggests that the reconfiguration is primarily complete following the completion of the third orbit.

The LROE control approach successfully reconfigures between a planar-elliptic relative orbit and lead–follower configurations. Otherwise, infeasible with the classic CW form, the modified LROE form provides no singularities in the transfer space. An analysis of Fig. 5 reveals that the along-track offset is first corrected before the ellipse scaling factor A_1. Further analysis of the Lagrangian brackets should reveal a greater sensitivity to the along-track position and the radial offset influence than the elliptic scaling factors.

VIII. Conclusions

The LROE variational equations are developed for nonsingular invariants of motion of the rectilinear Clohessy–Wiltshire (CW) solution. Because the LROEs provide a strong geometric insight, they are a useful tool to analyze how a perturbation impacts the relative trajectory geometry. This is illustrated through an atmospheric drag example. An LROE-based continuous feedback control is presented to illustrate the simplicity of setting up relative-orbit shape control to servo on a set of reference LROE states. Future work will consider LROE-based impulsive control methods, as well as expanding the LROE kinematics to the curvilinear CW formulation.

Acknowledgments

The authors would like to thank the NASA Space Technology Research Fellowship program, grant number NNX14AL62H, for support of this research. The authors also would like to thank Simon D'Amico for discussions on these new linearized-relative-orbit-element formulations and relative-orbit-element naming conventions.

References

[1] Woellert, K., Ehrenfreunda, P., Riccob, A. J., and Hertzfelda, H., "CubeSats: Cost-Effective Science and Technology Platforms for Emerging and Developing Nations," *Advances in Space Research*, Vol. 47, No. 4, Feb. 2011, pp. 663–684. doi:10.1016/j.asr.2010.10.009

[2] Roscoe, C. W. T., Westphal, J. J., Griesbach, J. D., and Schaub, H., "Formation Establishment and Reconfiguration Using Differential Elements in J2-Perturbed Orbits," *Journal of Guidance, Control, and Dynamics*, Vol. 38, No. 9, Sept. 2015, pp. 1725–1740. doi:10.2514/1.G000999

[3] Roscoe, C. W. T., Westphal, J. J., Lutz, S., and Bennett, T., "Guidance, Navigation, and Control Algorithms for CubeSat Formation Flying," *38th AAS Guidance and Control Conference*, AAS Paper 15-113, Jan.–Feb. 2015.

[4] Kitamura, S., "Large Space Debris Reorbiter Using Ion Beam Irradiation," *61st International Astronautical Congress*, Paper IEPC-2011-087, Sept.–Oct. 2010.

[5] Bombardelli, C., Urrutxua, H., Merino, M., Ahedo, E., Pelaez, J., and Olympio, J., "Dynamics of Ion-Beam Propelled Space Debris," *International Symposium on Space Flight Dynamics*, Feb.–March 2011.

[6] Kitamura, S., Hayakawa, Y., Nitta, K., Kawamoto, S., and Ohkawa, Y., "A Reorbiter for Large Geo Debris Objects Using Ion Beam Irradiation," *63rd International Astronautical Congress*, IAC Paper 2012-A6.7.10, Oct. 2012.

[7] Bombardelli, C., and Pelaez, J., "Ion Beam Shepherd for Contactless Space Debris Removal," *Journal of Guidance, Control, and Dynamics*, Vol. 34, No. 3, May–June 2011, pp. 916–920. doi:10.2514/1.51832

[8] Gómez, N. O., and Walker, S. J., "Eddy Currents Applied to De-Tumbling of Space Debris: Analysis and Validation of Approximate Proposed Methods," *Acta Astronautica*, Vol. 114, Sept.–Oct. 2015, pp. 34–53. doi:10.1016/j.actaastro.2015.04.012

[9] Schaub, H., and Moorer, D. F., "Geosynchronous Large Debris Reorbiter: Challenges and Prospects," *Kyle T. Alfriend Astrodynamics Symposium*, AAS Paper 2010-311, May 2010.

[10] Bennett, T., Stevenson, D., Hogan, E., McManus, L., and Schaub, H., "Prospects and Challenges of Touchless Debris Despinning Using Electrostatics," *Advances in Space Research*, Vol. 56, No. 3, Aug. 2015, pp. 557–568. doi:10.1016/j.asr.2015.03.037

[11] Hogan, E., and Schaub, H., "Space Weather Influence on Relative Motion Control Using the Touchless Electrostatic Tractor," *AAS/AIAA Spaceflight Mechanics Meeting*, AAS Paper 2014-425, Jan. 2014.

[12] Hogan, E., and Schaub, H., "Relative Motion Control for Two-Spacecraft Electrostatic Orbit Corrections," *Journal of Guidance, Control, and Dynamics*, Vol. 36, No. 1, Jan.–Feb. 2013, pp. 240–249. doi:10.2514/1.56118

[13] Schaub, H., and Jasper, L. E. Z., "Circular Orbit Radius Control Using Electrostatic Actuation for 2-Craft Configurations," *AAS/AIAA Astrodynamics Specialist Conference*, AAS Paper 2011-498, July–Aug. 2011.

[14] Ogilvie, A., Allport, J., Hannah, M., and Lymer, J., "Autonomous Satellite Servicing Using the Orbital Express Demonstration Manipulator System," *Proceedings of the 9th International Symposium on Artificial Intelligence, Robotics and Automation in Space (i-SAIRAS'08)*, Hollywood, CA, Feb. 2008, pp. 25–29.

[15] Amico, S. D., Ardaens, J. S., and Larsson, R., "In-Flight Demonstration of Formation Control Based on Relative Orbit Elements," *4th International Conference on Spacecraft Formation Flying Mi ssions and Technologies*, Aug. 2011.

[16] Schwartz, J., and Krenzke, T., "Error-Contracting Impulse Controller for Satellite Cluster Flight Formation," *AIAA Guidance, Navigation, and Control Conference*, AIAA Paper 2013-4541, Aug. 2013. doi:10.2514/6.2013-4541

[17] Chalt, S., and Spencer, D. A., "PROX-1: Automated Trajectory Control for On-Orbit Inspection," *37th Annual American Astronautical Society Guidance and Control Conference*, AAS Paper 14-066, Jan. 2014.

[18] Schaub, H., Vadali, S. R., and Alfriend, K. T., "Spacecraft Formation Flying Control Using Mean Orbit Elements," *Journal of the Astronautical Sciences*, Vol. 48, No. 1, 2000, pp. 69–87.

[19] Schaub, H., and Alfriend, K. T., "Impulsive Feedback Control to Establish Specific Mean Orbit Elements of Spacecraft Formations," *Journal of Guidance, Control, and Dynamics*, Vol. 24, No. 4, July–Aug. 2001, pp. 739–745. doi:10.2514/2.4774

[20] Vallado, D. A., "Orbital Mechanics Fundamentals," *Encyclopedia of Aerospace Engineering*, Wiley, Dec. 2010.

[21] Montebruck, O., Kirschner, M., and D'Amico, S., "E/I-Vector Separation for GRACE Proximity Operations," DLR, German Aerospace Center/German Space Operations Center TN 04–08, Dec. 2004.

[22] Gill, E., D'Amico, S., and Montenbruck, O., "Autonomous Formation Flying for the PRISMA Mission," *Journal of Spacecraft and Rockets*, Vol. 44, No. 3, May–June 2007, pp. 671–681. doi:10.2514/1.23015

[23] Clohessy, W. H., and Wiltshire, R. S., "Terminal Guidance System for Satellite Rendezvous," *Journal of the Aerospace Sciences*, Vol. 27, No. 9, Sept. 1960, pp. 653–658. doi:10.2514/8.8704

[24] Chavez, F. R., and Lovell, T. A., "Relative-Orbit Element Estimation for Satellite Navigation and Guidance," *AIAA/AAS Astrodynamics Specialist Conference and Exhibit*, AIAA Paper 2004-5214, Aug. 2004.

[25] Lovell, T. A., and Tragesser, S. G., "Guidance for Relative Motion of Low Earth Orbit Spacecraft Base on Relative Orbit Elements," *AIAA/AAS Astrodynamics Specialist Conference*, AIAA Paper 2004-4988, Aug. 2004.

[26] Lovell, T. A., Tragesser, S. G., and Tollefson, M. V., "A Practical Guidance Methodology for Relative Motion of LEO Spacecraft Base on the Clohessy–Wiltshire Equations," *14th AAS/AIAA Spaceflight Mechanics Meeting*, AAS Paper 04-252, Feb. 2004.

[27] Amico, S. D., Gill, E., and Montenbruck, O., "Relative Orbit Control Design for the PRISMA Formation Flying Mission," *AIAA Guidance, Navigation, and Control Conference and Exhibit*, AIAA Paper 2006-6067, Aug. 2006. doi:10.2514/6.2006-6067

[28] Bevilacqua, R., and Lovell, T. A., "Analytical Guidance for Spacecraft Relative Motion Under Constant Thrust Using Relative Orbit Elements," *Acta Astronautica*, Vol. 102, Sept.–Oct. 2014, pp. 47–61. doi:10.1016/j.actaastro.2014.05.004

[29] Lovell, T. A., and Spencer, D. A., "Relative Orbital Elements Formulation Based upon the Clohessy–Wiltshire Equations," *Journal of Astronautics*, Vol. 61, No. 4, 2014, pp. 341–366. doi:10.1007/s40295-014-0029-6

[30] D'Amico, S., "Relative Orbital Elements as Integration Constants of Hill's Equations," German Space Operations Center (DLR/GSOC) TN 05-08, Dec. 2005.

[31] Schaub, H., and Alfriend, K. T., "Hybrid Cartesian and Orbit Element Feedback Law for Formation Flying Spacecraft," *Journal of Guidance, Control, and Dynamics*, Vol. 25, No. 2, March–April 2002, pp. 387–393. doi:10.2514/2.4893

[32] Gim, D.-W., and Alfriend, K. T., "The State Transition Matrix of Relative Motion for the Perturbed Non-Circular Reference Orbit," *Journal of Guidance, Control, and Dynamics*, Vol. 26, No. 6, 2003, pp. 956–971. doi:10.2514/2.6924

[33] Schaub, H., "Relative Orbit Geometry Through Classical Orbit Element Differences," *Journal of Guidance, Control, and Dynamics*, Vol. 27, No. 5, Sept.–Oct. 2004, pp. 839–848. doi:10.2514/1.12595

[34] D'Amico, S., and Montenbruck, O., "Proximity Operations of Formation-Flying Spacecraft Using an Eccentricity/Inclination Vector Separation," *Journal of Guidance, Control, and Dynamics*, Vol. 29, No. 3, 2006, pp. 554–563. doi:10.2514/1.15114

[35] Ichimura, Y., and Ichikawa, A., "Optimal Impulsive Relative Orbit Transfer Along a Circular Orbit," *Journal of Guidance, Control, and Dynamics*, Vol. 31, No. 4, July–Aug. 2008, pp. 1014–1027. doi:10.2514/1.32820

[36] Spencer, D. A., "Relative Orbit Targeting Using Artificial Potential Functions," *AAS/AIAA Space Flight Mechanics Meeting*, AAS Paper 2016-204, Feb. 2016.

[37] Spencer, D. A., "Automated Trajectory Control for Proximity Operations Using Relative Orbital Elements," Ph.D. Dissertation, Georgia Inst. of Technology, Atlanta, GA, May 2015.

[38] Schaub, H., and Junkins, J. L., *Analytical Mechanics of Space Systems*, 2nd ed., AIAA Education Series, AIAA, Reston, VA, Oct. 2009, pp. 561–612.

[39] Vallado, D. A., *Fundamentals of Astrodynamics and Applications*, 4th ed., Microcosm Press, March 2013, pp. 388–419.

[40] Ilgen, M. R., "Low Thrust OTV Guidance Using Lyapunov Optimal Feedback Control Techniques," *Astrodynamics, Vol. 85, Advances in the Astronautical Sciences Series*, Springer, Berlin, 1993, pp. 1527–1546; also AAS Paper 1993-680, 1993.

[41] Battin, R. H., *An Introduction to the Mathematics and Methods of Astrodynamics*, AIAA Education Series, AIAA, New York, 1987.

[42] Bennett, T., Schaub, H., and Roscoe, C. W. T., "Faster-than-Natural Spacecraft Circumnavigation via Way Points," *Acta Astronautica*, Vol. 123, June–July 2016, pp. 376–386. doi:10.1016/j.actaastro.2016.01.025

[43] Hogan, E., and Schaub, H., "Space Debris Reorbiting Using Electrostatic Actuation," *AAS Guidance and Control Conference*, AAS Paper 2012-016, Feb. 2012.